Molecular Dynamics Simulations of the Nucleation of Water: Determining the Sticking Probability and Formation Energy of a Cluster

Kyoko K. Tanaka,[1, a)] Akio Kawano,[2] and Hidekazu Tanaka[1]
[1)] *Institute of Low Temperature Science, Hokkaido University, Sapporo 060-0819, Japan*
[2)] *Japan Agency for Marine-Earth Science and Technology, Kanagawa, Japan*

(Dated: 9 January 2022)

We performed molecular dynamics (MD) simulations of the nucleation of water vapor in order to test nucleation theories. Simulations were performed for a wide range of supersaturation ratios (S = 3-25) and water temperatures (T_w = 300-390 K). We obtained the nucleation rates and the formation free energies of a subcritical cluster from the cluster size distribution. The classical nucleation theory (CNT) and the modified classical nucleation theory (MCNT) overestimate the nucleation rates in all cases. The semi-phenomenological (SP) model, which corrects the MCNT prediction using the second virial coefficient of a vapor, reproduces the formation free energy of a cluster with the size $\lesssim$ 20 to within 10 % and the nucleation rate and cluster size distributions to within one order of magnitude. The sticking probability of the vapor molecules to the clusters was also determined from the growth rates of the clusters. The sticking probability rapidly increases with the supersaturation ratio S, which is similar to the Lennard-Jones system.

Keywords: water, molecular dynamics method, nano-clusters, nucleation, phase transitions, liquid-vapour transformations, sticking probability

arXiv:1401.1899v2 [physics.chem-ph] 26 Feb 2014

I. INTRODUCTION

The classical nucleation theory (CNT) is the most widely used model for describing homogeneous nucleation and provides the nucleation rate as a function of the supersaturation ratio and the surface tension of a condensed phase[1–4]. However, many studies have reported that the CNT fails to describe experimentally obtained results[5–27]. In the case of water, the deviations between the nucleation rates predicted by the classical nucleation theory and the experimental values are in the order of 10^2-10^{36}[13,18,20–27]. The nucleation rates obtained by molecular dynamics (MD) and Monte Carlo (MC) simulations also significantly differ from the predictions of the CNT[28–49]. The nucleation rate is governed by the formation free energy of a critical cluster, which is the smallest thermodynamically stable cluster. In the classical nucleation theory, the formation free energy is simply evaluated using the surface energy of the bulk material. Since the critical clusters are considered to be nano-sized, the error in the classical theory is thought to come from the difference in the properties of such a small cluster and a bulk material.

In previous studies, there have been significant advances in theoretical models of homogeneous nucleation[9,10,12,14,40,50–55]. One of the most successful and useful models is the semi-phenomenological (SP) model[9,12,14], which corrects the evaluation of the formation energy of a cluster in the CNT by using the second virial coefficient of a vapor. The predictions of the SP model agree well with experimental data for various substances including water[9,12,14]. By performing MD simulations of nucleation for Lennard-Jones systems, Tanaka et al.[46,48] tested the SP model and found that it also agrees well with their MD simulations. However, only large supersaturation ratios were possible in their MD simulations. Recent large scale simulations by Diemand et al.[49] found some deviations in the nucleation rate from the SP model in the case of a small supersaturation ratio.

Besides Lennard-Jones systems, many other MD simulations examining the nucleation process of water molecules have been carried out. Yasuoka and Matsumoto[31] investigated homogeneous nucleation for the first time using MD simulations of water molecules. The nucleation rate they obtained at 350 K was two orders of magnitude less than that predicted by the classical theory. Matsubara et al.[47] carried out MD simulations at various temperatures and supersaturation ratios, using a simple point charge/extended (SPC/E) water model[56]. They measured the nucleation rate, the critical nucleus size, and the formation free energy of a cluster and compared them with the various theoretical models. They showed that all theoretical models (CNT, SP model, and the scaled model) predict the nucleation rates obtained by the simulations to within one or two orders of magnitude. On the other hand, the formation free energy of a cluster derived by the simulations was considerably larger than that obtained with the theoretical models. They showed that the deviations in the formation free energy can be explained by the larger growth rate of clusters than that assumed by the theories. Recently, Zipoli et al.[57] developed a new coarse-grained model for water to study nucleation from the vapor and obtained smaller nucleation rates than the previous studies.

In addition to the formation free energy of a cluster,

[a)] Electronic mail: kktanaka@lowtem.hokudai.ac.jp

the sticking probability α of vapor molecules to clusters is another important factor for determining the nucleation rate. The sticking probability is usually assumed to be unity, despite the fact that the nucleation rate is proportional to α in the nucleation theory. In the previous studies[48,49], the sticking probability in a Lennard-Jones type system was examined through MD simulations, by observing the growth rate of stable clusters larger than the critical size. They showed that the sticking probability decreases with decreasing supersaturation ratio; however, the validity of their findings has not been confirmed. Therefore, it is worthwhile investigating the sticking probability for various materials.

In the present study, we performed MD simulations of water molecules for a wide range of initial supersaturation ratios and temperatures. We observed the nucleation rates and derived the formation free energy by using the size distribution of the clusters. By comparing these numerical results with theories, we can test the theoretical models. We also obtained the sticking probability from the MD simulations based on the previous method[48,49]. In Section II, we describe the numerical procedure for our MD simulations, and in Section III we present our numerical results and compare the numerical results with the theories. We also determine the sticking probability and the dependence of the supersaturation ratio. In Section IV, we summarize the results of the present study.

II. NUMERICAL PROCEDURE AND ANALYSIS

We performed simulations of the nucleation process in systems of 4,000 of water molecules, using the SPC/E rigid water model[56]. We assumed NVT (constant volume and temperature) ensembles and used a three-dimensional periodic boundary condition. Initially, the molecules are located randomly without being overlapped with others and the system is relaxed to be in the equilibrium state at 1000 K. Using this initial condition, we started the simulations. In our simulations, the number of water molecules was not so large. In order to improve the statistical accuracy, we performed 20 runs with different initial positions and velocities of molecules for each parameters of temperature T and initial supersaturation ratio S_0. The time step was set as 2.0 fs. The total number of time steps was (4-10) $\times 10^6$ in each run. The simulation box contained 4000 water molecules and 4000 (or 8000) argon carrier gas molecules to control the temperature. To compute the long-range electrostatic interactions, we adopted the reaction field-zero method[58] in which a dielectric constant of infinity and a group-based cutoff are employed. In this study we set the cutoff radius to 3.5 nm.

The computational region is a cube with periodic boundaries. By varying the box size L, we set the initial number density of molecules or the initial supersaturation ratio S_0. The supersaturation ratio is defined as $S = P_1/P_{\rm sat}$, where P_1 and $P_{\rm sat}$ are the partial pressure of the monomers and the pressure in a saturated vapor. The resulting supersaturation is approximately given by $S = P_{\rm total}/P_{\rm sat}$ with the total pressure $P_{\rm total}$ because of small amount of clusters larger than dimers. Simulations were performed for various temperatures and supersaturation ratios, *i.e.,* T = 250-375 K and S = 3-25. The parameter sets for each run are shown in Table I. 28 parameter sets were chosen, so that the total number of simulations is 560. For a sufficiently high supersaturation ratio, the simulation gives a very large nucleation rate and the number of the vapor molecules decreases so quickly. In such a case, a steady nucleation with a constant supersaturation ratio is not realized. In our simulations, in order to observe steady nucleation, we chose lower supersaturation ratios compared with the previous study[47]. For the interaction between carrier gas and water, we used the potential of the Lennard-Jones type:

$$V(r) = 4\varepsilon[(\sigma/r)^{12} - (\sigma/r)^6], \tag{1}$$

where r is the distance between argon and oxygen and the parameters σ and ε are given by $\sigma = \sqrt{\sigma_{\rm Ar}\sigma_{\rm O}}$ and $\varepsilon = \sqrt{\varepsilon_{\rm Ar}\varepsilon_{\rm O}}$ with $\sigma_{\rm Ar} = 3.40\mathring{A}$, $\sigma_{\rm O} = 3.17\mathring{A}$, $\varepsilon_{\rm Ar} = 0.979$ kJ mol^{-1}, and $\varepsilon_{\rm O} = 0.652$ kJ mol^{-1}[59]. The carrier gas temperature T was controlled directly with a Nosé-Hoover thermostat, while the temperature of the water was controlled indirectly through interaction with the carrier gas molecules. The temperature of the water molecules $T_{\rm w}$ deviates from the temperature of the carrier gas because of the latent heat effect that results from condensation formation. We defined clusters using the bonding criterion that the interaction energy of a molecular pair is less than -10 kJ/mol[47].

We obtained the nucleation rate and compared the number density of clusters based on the same method as in the previous studies[48,49]. We also derived the formation free energies from the cluster size distribution[60]. To derive the formation free energy of a cluster ΔG_i, where i is the number of molecules in the cluster, we use the relation between the equilibrium size distribution $n_{\rm e}(i)$ and the formation free energy of a cluster ΔG_i[48,49]:

$$\frac{\Delta G_i}{kT} = \ln\left(\frac{n(1)}{n_{\rm e}(i)}\right), \tag{2}$$

where $n(1)$ is the number density of the monomers.

The steady nucleation rate J is the net number of the transition from i-mer to $i+1$-mer and given by

$$J = R^+(i)n(i) - R^-(i+1)n(i+1), \tag{3}$$

where $R^+(i)$ is the transition rate from a cluster of i molecules, i-mer, to (i+1)-mer per unit time, *i.e.,* the accretion rate, and $R^-(i)$ is the transition rate from i-mer to (i-1)-mer per unit time, *i.e.,* the evaporation rate of i-mer. $R^+(i)$ is given by

$$R^+(i) = \alpha n(1) v_{\rm th}(4\pi r_0^2 i^{2/3}), \tag{4}$$

where $v_{\rm th}$ is the thermal velocity, $\sqrt{kT/2\pi m}$, and r_0 is the radius of a monomer, $(3m/4\pi\rho_{\rm m})^{1/3}$ where m is the mass of a molecule and $\rho_{\rm m}$ is the bulk density. The evaporation rate is obtained from the principle of detailed balance in thermal equilibrium.

$$R^-(i+1)n_{\rm e}(i+1) = R^+(i)n_{\rm e}(i). \tag{5}$$

From Eqs.(4) and (5), we have

$$J = R^+(i)n(i) - R^+(i)n_{\rm e}(i)\frac{n(i+1)}{n_{\rm e}(i+1)}, \tag{6}$$

which leads to

$$\frac{n_{\rm e}(i)}{n(i)} = \frac{n_{\rm e}(i-1)}{n(i-1)}\left(1 - \frac{J}{R^+(i-1)n(i-1)}\right)^{-1}. \tag{7}$$

Equation (7) shows $n_{\rm e}(i)$ agrees well with the number density of the clusters $n(i)$ obtained by the MD simulations for subcritical clusters $i \leq i^*$, because $J \ll R^+(i)n(i)$ for $i \leq i^*$. From Eq.(7), we obtain $n_{\rm e}(i)$ if $J, n(i)$ and $n_{\rm e}(i-1)$ are given. For example $n_{\rm e}(2)$ is obtained by $J, n(2)$, and $n_{\rm e}(1)[= n(1)]$. Also for a larger i, we can obtain $n_{\rm e}(i)$ recursively. Matsubara et al.[47] calculated the equilibrium number density, using the different formula derived by Yasuoka and Matsumoto[30] from Fokker-Plank equation. Our formula leads to the same as Matsubara et al.[47] for $i^* >> 1$ (see Appendix).

In the theoretical models, the formulae for ΔG_i are given by

$$\frac{\Delta G_{\rm CNT,i}}{kT} = -i\ln S + \eta i^{2/3},$$
$$\frac{\Delta G_{\rm MCNT,i}}{kT} = -(i-1)\ln S + \eta(i^{2/3}-1),$$
$$\frac{\Delta G_{\rm SP,i}}{kT} = -(i-1)\ln S + \eta(i^{2/3}-1) + \xi(i^{1/3}-1), \tag{8}$$

where $\Delta G_{\rm CNT,i}$, $\Delta G_{\rm MCNT,i}$, and $\Delta G_{\rm SP,i}$ are the formation free energies of a cluster in the CNT, the modified CNT (MCNT), and the SP model, respectively, and η and ξ are parameters determined by the bulk surface energy and second virial coefficient[48,49]. In the classical theory, there is a theoretical inconsistency in the S dependence. Consequently the MCNT has often been used. In the next section, we compare the CNT, MCNT and SP models with the our numerical results. Although there are some differences between the thermodynamic quantities obtained by using SPC/E force and those by experiments of real water, we should use those of SPC/E force for the consistency to the model. For thermodynamic quantities such as the surface tension and the saturated vapor pressure of the SPC/E water, we use the same data as Matsubara et al.[47]

III. RESULTS

A. A typical case

Let $N(> i_{\rm th})$ denote the number of clusters larger than a threshold size $i_{\rm th}$. Based on Yasuoka and Matsumoto method[30], we can obtain the nucleation rate from $N(> i_{\rm th})$. Figure 1 shows time evolution of the supersaturation ratio and the number of clusters, $N(> i_{\rm th})$, in a typical case where $T = 350$ K and $S_0 = 6.67$ (run 5d in Table I). Note that $N(> i_{\rm th})$ is averaged over 20 runs with different initial positions and velocities of molecules. In Figure 1, we plot $N(> i_{\rm th})$ for $i_{\rm th}$ =20, 30, and 40.

The threshold $i_{\rm th}$ should be larger than the critical size i^* for the evaluation of the nucleation rate. In this case, the critical size i^* is estimated to be 14 (or 7) with the SP (or CNT) model. In this figure, the number of stable nuclei $N(> i_{\rm th})$ increases almost linearly in the period of $t = (6-12)$ns. From the slope, the nucleation rate is measured with $J(= \dot{N}[> i_{\rm th}]/L^3)$. In the evaluation of J, we chose the slope between the times at $N(> i_{\rm th}) = 2$ and 4, *e.g.,* $t = 8-10$ ns for $i_{\rm th}$=20. Then, the nucleation rate is obtained as 8.92×10^{24}, 7.37×10^{24}, and 6.19×10^{24}cm^{-3}s^{-1}, for $i_{\rm th} = 20$, 30, and 40, respectively. In this evaluation of the nucleation rate, uncertainties of 20-30% exist, depending on the choice of $i_{\rm th}$ and the time interval.

During this period of $t =$ (8-10) ns, the average value of the supersaturation S and the temperature of the water molecules $T_{\rm w}$ were 4.7 and 361 K, respectively. Using these values, we can calculate J predicted by the theoretical models. In the MCNT, the CNT and the SP models, the nucleation rate are obtained as 1.5×10^{27}, 8.0×10^{25}, and $J = 2.1 \times 10^{24}$cm^{-3}s^{-1}, respectively. The prediction of the SP model is much closer to the values obtained in the MD simulations than the MCNT and the CNT.

B. Nucleation rate

Fig. 2 shows the time evolutions of $N(> i_{\rm th})$ for $i_{\rm th} =$ 20, 30, and 40 in the various runs (6e, 5c, 3c and 2e). We evaluate the nucleation rates from the slopes between the times at $N(> i_{\rm th}) = 2$ and $N(> i_{\rm th}) = 4$ for all runs except run 6e. For run 6e, we use the slope between the times at $N(> i_{\rm th}) = 1$ and 3 because of the small number of clusters. The nucleation rates obtained in all MD simulations are listed in Table II, where we chose $i_{\rm th}$ =20 for all runs because the size of critical cluster is estimated to be less than 20 for all runs (see Section III.D). As stated in the previous section, there are some uncertainties in the estimation of the nucleation rates. So we include the errors in the nucleation rates in Table II.

Fig. 3 shows the nucleation rates obtained by the MD simulations as a function of the supresaturation ratio

for various temperatures. The previous results are also shown: crosses and triangles are the results by Matsubara et al.[47] and Zipoli et al.[57], respectively. The nucleation rates by SP model (solid curves) are also plotted. The obtained nucleation rates are about one-order-of-magnitude smaller than Matsubara et al.[47] because of the smaller supersaturation ratios. We find good agreements between the MD simulations and the SP model within one-order-of-magnitude in the cases of low temperatures for both our runs and the previous results.

Figure 4 shows the ratios of the nucleation rates in the MD simulations (at $T_{\rm w}$) to the rates obtained with the theoretical models. The results are plotted with circles for the SP model, triangles for the MCNT, and crosses for the CNT. The nucleation rates predicted by the SP model are within one order of magnitude of the MD simulations, whereas the nucleation rates predicted by the CNT and MCNT are much larger than the MD simulations. We also plotted the ratios $J_{\rm MD}/J_{\rm SP}$, by using results by Matsubara et al.[47] (i.e., data in Table I in[47]). Our results agree well with theirs. The ratio of $J_{\rm MD}/J_{\rm SP}$ gradually increases with temperature in both results. The nucleation rates obtained with the theoretical models are also listed in Table II.

In Figure 4, we also show the results of the Lennard-Jones system[48] for reference. The SP model also predicts the nucleation rates to within one order of magnitude for the Lennard-Jones system, although the supersaturation ratios are limited to be small. In the case of the Lennard-Jones system, the CNT considerably underestimates the nucleation rates (*i.e.,* the $J_{\rm MD}/J_{\rm CNT}$ ratio is much larger than 10^9) at $T < 0.4(\varepsilon/k_{\rm B})$, where ε and $k_{\rm B}$ are the depth of the Lennard-Jones potential and the Boltzmann constant, respectively. On the other hand, the CNT predictions agree with the nucleation rates obtained by the MD simulations to within two orders of magnitude in the case of water.

In Fig. 5, we show the nucleation rates as a function of $\ln S/(T_c/T-1)^{1.5}$ in order to compare our results with the scaling relation proposed by Hale[61]. The data by the MD simulations and the theoretical predictions are the same as those in Fig. 3. For the MD simulations using SPC/E water model, we set $T_c = 630$ K for the consistency to the model[47]. We also put the experimental data for water nucleation[6,20,22,23,26,27]. For the experimental results and Zipoli et al.[57], T_c is set to be 647 K[20]. From Fig. 5, J seems to be scaled by $\ln S/(T_c/T-1)^{1.5}$, but is not proportional to it.

C. Cluster size distributions

Figure 6 shows the size distributions $n(i)$ obtained from 8 runs at various temperatures $T_{\rm w}$ and initial supersaturation ratios. For each temperature, we show high-S cases (right column) and low-S cases (left column). The MCNT significantly overestimates the distributions (by factors 10^3). In all cases, the SP model predicts the size distributions more accurately than both the MCNT and the CNT for clusters smaller than the critical size. At $i = 2$ the SP model agrees perfectly with the MD simulations in all cases. However, the SP model disagrees with the results of the MD simulations for large clusters. There is also a relatively large deviation at $i = 4$. This is due to the stable four-ring structure[54,62]. These results for the size distributions are consistent with the nucleation rate, as shown Section II.B.

D. Formation free energy

We derive the formation free energy of a cluster $\Delta G_i(S)$, using the equilibrium size distribution $n_{\rm e}(i)$ given by Eq.(7). In the derivation, we use the nucleation rate J and $n(i)$ obtained by the MD simulations and $R^+(i)$, where we use the value of α measured by the simulations (see Section II.E. and Table II.) Using the S-dependence of ΔG_i in Eq.(8) except the CNT, we also obtain ΔG_i at $S = 1$ as

$$\Delta G_i(S=1) = \Delta G_i(S) + (i-1)kT\ln S, \qquad (9)$$

where ΔG_i is obtained from Eq.(2). $\Delta G_i(S=1)$ corresponds to the contribution of the surface effect to the formation free energy of a cluster. If we know $\Delta G_i(S=1)$, we can predict ΔG_i and the nucleation rate for any value of S.

Fig. 7 shows the size distribution of clusters obtained by MD simulations and the equilibrium one in run 5d. The formation free energies ΔG_i are shown for $S = 4.7$ and $S = 1$ in Fig. 7. From ΔG_i for $S = 4.7$, we obtain the maximum value of the formation free energy and the size of the critical cluster in run 5d, *i.e.,* $\Delta G_i^* = 7.0kT$ and $i_* = 12$. Table II shows the sizes of critical cluster obtained by the simulations for all runs.

In Fig. 8, we compare the maximum value of the formation free energy at the critical cluster between the theoretical models and the MD simulations for all runs. Evaluating ΔG_i^* in the theoretical model, we use the values of the temperature $T_{\rm w}$ and the supersaturation ratio obtained by the simulations shown in Table II. The CNT and MCNT considerably underestimate the maximum free energies. The SP model predicts the maximum free energies to a higher accuracy than the CNT and MCNT: the SP model predicts the maximum free energies within 30 %. In Matsubara et al.[47], the similar comparison was performed. There are some differences between the our results and[47]. We confirmed that there is an inconsistency in Matsubara et al.[47] where they used slightly smaller temperatures in their figures than the true values of $T_{\rm w}$ in Table I.[47] (private communications).

Figure 9 shows the formation free energy $\Delta G_i(S=1)$ obtained by simulations at various temperatures. Predictions of the theoretical models are plotted with solid lines

(SP model) and dashed lines (MCNT). The SP model exhibits much better agreement with the numerical results than the MCNT. The SP model reproduces the formation free energy of a cluster to within 10 %. The CNT also reproduces the formation free energy of a cluster better than the MCNT, but the gradient of the CNT data is different to the numerical results.

From ΔG_i obtained by MD simulations, we can calculate the nucleation rate by using

$$J = \left\{ \sum_{i=1}^{\infty} \frac{1}{R^+(i) n_{\rm e}(i)} \right\}^{-1}, \tag{10}$$

where $n_{\rm e}(i)$ is given by Eq.(2). We confirmed the nucleation rates given by Eq.(10) predict $J_{\rm MD}$ measured by the MD simulations within the accuracy of 1 % for all runs.

E. Sticking probability

As shown in Section II, the nucleation rate is obtained from the equilibrium number density $n_e(i)$ and the accretion rate which is proportional to the sticking probability α. Using the growth rate of stable clusters obtained in the present MD simulation, we evaluated the sticking probability.

Tanaka et al.[48] evaluated the sticking probability from the growth rate of stable clusters, di/dt, neglecting the effect of evaporation. In the present study the evaporation effect was taken into account based on the method of Diemand et al.[49]. The growth rate of clusters, di/dt, is given by

$$\frac{di}{dt} = R^+(i) - R^-(i). \tag{11}$$

From Eqs.(4) and (5), we have

$$\frac{di}{dt} = 4\pi r_0^2 i^{2/3} \alpha n(1) v_{\rm th} \left[1 - \left(\frac{i-1}{i} \right)^{2/3} e^{\frac{\Delta G_i - \Delta G_{i-1}}{kT}} \right] \tag{12}$$

where we use $n_{\rm e}(i) = n(1) \exp[-\Delta G_i/(kT)]$.

As shown in Eq.(8), ΔG_i has a bulk term ($\propto i$) and a surface term ($\propto i^{2/3}$). Since the other terms in Eq.(8) are smaller than these terms, the sum, $\Delta G_i + ikT \ln S$ is approximately proportional to $i^{2/3}$ and

$$\Delta G_i - \Delta G_{i-1} \simeq -kT \ln S \tag{13}$$

for $i \gg 1$. Hence for $i \gg 1$, we obtain

$$\frac{di}{dt} = \alpha n(1) v_{\rm th} (4\pi r_0^2 i^{2/3}) \left[1 - \frac{1}{S} \right]. \tag{14}$$

Equation (14) suggests that the evaporation becomes considerable when the supersaturation ratio is small. Accordingly, the sticking probability is given by

$$\alpha = \frac{3}{4\pi r_0^2 v_{\rm th} n(1)} \left(1 - \frac{1}{S} \right)^{-1} \frac{di^{1/3}}{dt}. \tag{15}$$

The time derivative of $i^{1/3}$ was evaluated from the MD simulations. Figure 10 shows the time derivative of $i^{1/3}$ for run 5d. Based on the slope, the sticking probability was measured to be 0.472. Using Eq.(15), we obtained the sticking probability for all runs. The values of α are also listed in Table II. The results are shown in Figure 11 (a) as a function of supersaturation rate. By plotting a line of best fit, we obtained an empirical formula for the sticking probability:

$$\ln \alpha = 1.16 \ln S \left(\frac{T}{273{\rm K}} \right)^{3.3} - 5.3 \tag{16}$$

(see Fig. 11 (b)). The sticking probability increases with the supersaturation ratio, which is consistent with the Lennard-Jones system[48,49]. The formula (16) is valid within the parameter range of S in which our MD simulations are done. In this range ($S > 3$), Eq.(16) indicates that α increases with the temperature for a fixed S. In the case of the flat surface and the equilibrium state ($S = 1$), on the other hand, the decreasing of α with the increasing temperature is reported by the previous study[63]. Around the equilibrium state ($S \simeq 1$), the sticking probability should be examined in the future work.

We evaluated α, by using the growth rate of clusters larger than the critical size with Eq.(15). Matsubara et al.[47] evaluated the sticking probability (or the sticking coefficient), by directly measuring the condensation flux (*i.e.,* accretion rate) for clusters smaller than or comparable to the critical size instead of the growth rate. Their values are one-order-of-magnitude greater than ours. This would indicate that the sticking probability might be different between the under-critical and the over-critical sizes. Matsubara et al.[47] suggested that their large sticking coefficients are due to the large surface area of clusters. For small clusters, larger surface areas than the simple prediction with the bulk density are also reported by other studies[30,64]. A high supersaturation ratio in Matsubara et al.[47] can be another factor which causes the above difference in α.

IV. SUMMARY AND FUTURE WORK

Our results on the nucleation of water molecules are summarized as follows.

1. The cluster size distributions, the formation free energy of a cluster, and the nucleation rates obtained from the MD simulations are compared with the predictions by the theoretical models (see Figures 3-6 and Table II). The CNT and the MCNT overestimate the nucleation rates (or the number density of critical clusters) for all runs. On the other hand, the SP model gives a better prediction. The nucleation rates predicted by the SP model are within one order of magnitude. The free energy of cluster formation ΔG_i (or the cluster integrals) for small clusters ($i \lesssim 20$) is also well predicted by the

SP model (with 10% accuracy) for a wide range of temperature. In this study, only large supersaturation ratios and nucleation rates were considered. In order to verify the validity of the SP model for smaller supersaturation ratios, simulations using a larger number of molecules are necessary.

2. The sticking probability of vapor molecules onto clusters was measured in supersaturated conditions, by using the growth rate of stable clusters in the MD simulations. The sticking probability α increases with the supersaturation ratio. This tendency is the same as exhibited by the Lennard-Jones system[48,49]. The lowest value of α was observed to be 0.3 for $T \simeq 380$ K and $S \simeq 3.3$. It is expected that α would be much smaller than 0.3 for lower supersaturation ratios. For such low-S cases, we must estimate α precisely for the evaluation of J.

V. ACKNOWLEDGMENTS

We are grateful to Dr. Matsubara for discussions and valuable comments. H. Tanaka and K. K. Tanaka acknowledge Dr. Diemand and Dr. Angelil for fruitful discussions. We would like to thank the anonymous reviewers for their valuable suggestions to improve the quality of the paper. This work was supported by the Japan Society for the Promotion of Science (JSPS).

VI. APPENDIX

In the present paper, we use Eq.(7) to obtain the equilibrium number density. In this appendix, we show the relation Eq.(7) to the formula used in Matsubara et al.[47]. Equation (7) is a recurrence relation and yields

$$\frac{n_{\rm e}(i)}{n(i)} = \prod_{k=1}^{i-1}\left(1-\frac{J}{R^+(k)n(k)}\right)^{-1} = \prod_{k=1}^{i-1}\exp\left\{-\ln\left(1-\frac{J}{R^+(k)n(k)}\right)\right\}. \quad (17)$$

If we assume

$$\frac{J}{R^+(i)n(i)} \ll 1, \quad (18)$$

for all i, we obtain

$$\frac{n_{\rm e}(i)}{n(i)} = \prod_{k=1}^{i-1}\exp\left\{-\frac{J}{R^+(k)n(k)}\right\} = \exp\left\{-J\sum_{k=1}^{k-1}\frac{1}{R^+(k)n(k)}\right\} \quad (19)$$

which corresponds to the formula (27) in Matsubara et al[47]. Since the nucleation rate is expressed with the Zeldovich factor Z:

$$J \simeq R^+(i_*)n_{\rm e}(i_*)Z,$$
$$Z = \left\{\frac{-1}{2\pi kT}\left(\frac{d^2\Delta G_i}{di^2}\right)_{i=i_*}\right\}^{1/2}, \quad (20)$$

the condition (18) is written as

$$Z \ll 1. \quad (21)$$

In the theory of CNT, MCNT, and SP model, the Zeldovich factor is given by

$$Z = \frac{1}{3}i_*^{-2/3}\sqrt{\frac{\eta}{\pi}+\frac{\xi}{\pi}i_*^{-1/3}}, \quad (22)$$

where Z in the CNT (or MCNT) corresponds to the case of $\xi = 0$. Equation (22) indicates that the condition (18) is satisfied in the case of $i^* \gg (\eta/9\pi)^{3/4} \sim 1$.

[1] M. Volmer and A. Weber, Z. Phys. Chem. **119**, 277 (1926).
[2] V. R. Becker and W. Döring, Ann. Physik. **24**, 719 (1935).
[3] J. B. Zel'dovich, J. Exp. Theor. Phys. **12**, 525 (1942).
[4] J. Feder, K. C. Russell, J. Lothe, and G. M. Pound, Adv. in Phys. **15**, 111 (1966).
[5] J. L. Schmitt, G. W. Adams, and R. A. Zalabsky, J. Chem. Phys. **77**, 2089 (1982).
[6] R. C. Miller, R.J. Anderson, J. L. Kassner, Jr., and D. E. Hagen, J. Chem. Phys. **78**, 3204 (1983).
[7] J. L. Schmitt, R. A. Zalabsky, and G. W. Adams, J. Chem. Phys. **79**, 4496 (1983).
[8] G. W. Adams, J. L. Schmitt, and R. A. Zalabsky, J. Chem. Phys. **81**, 5074 (1984).
[9] A. Dillmann and G. E. A. Meier, J. Chem. Phys. **94**, 3872 (1991).
[10] D. W. Oxtoby, J. Phys. Condens. Matter **4**, 7627 (1992).
[11] D. Wright, R. Caldwell, C. Moxely, and M. S. ElShall, J. Chem. Phys. **98**, 3356 (1993).
[12] C. F. Delale and G. E. A. Meier, J. Chem. Phys. **98**, 9850 (1993).
[13] Y. Viisanen, R. Strey, and H. Reiss, J. Chem. Phys. **99**, 4680 (1993).
[14] A. Laaksonen, I. J. Ford, and M. Kulmala, Phys. Rev. E **49**, 5517 (1994).
[15] Y. Viisanen and R. Strey, J. Chem. Phys. **101**, 7835 (1994).
[16] D. Kane and M. S. El-Shall, J. Chem. Phys. **105**, 7617 (1996).
[17] K. Hämeri and M. Kulmala, J. Chem. Phys. **105**, 7696 (1996).
[18] C. C. M. Luijten, K. J. Bosschaart, and M. E. H. van Dongen, J. Chem. Phys. **101**, 8116 (1997).
[19] M. P. Anisimov, P. K. Hopke, I. N. Shaimordanov, S. D. Shandakov, and L-E. Magnusson, J. Chem. Phys. **115**, 810 (2001).
[20] J. Wölk, and R. Strey, J. Phys. Chem. B **105**, 11683 (2001).
[21] V. B. Mikheev, P. M. Irving, N. S. Laulainen, S. E. Barlow, and V. V. Pervukhin, J. Chem. Phys. **116**, 10772 (2002).
[22] A. Khan, C. H. Heath, U. M. Dieregsweiler, B. E. Wyslouzil, and R. Strey, J. Phys. Chem. B **119**, 3138 (2003).
[23] y. J. Kim, B. E. Wyslouzil, G. Wilemski, J. Wölk, and R. Strey, J. Phys. Chem. A **108**, 43658 (2004).
[24] V. Holten, D. G. Labetski, and M. E. H. van Dongen, J. Chem. Phys. **123**, 104505 (2005).
[25] D. Brus, V. Ždímal, and J. Smolík, J. Chem. Phys. **129**, 174501 (2008).
[26] D. Brus, V. Ždímal, and H. Uchtmann, J. Phys. Chem. A **131**, 074507 (2009).
[27] A. A. Manka, D. Brus, A-P. Hyvärinen, H. Lihavainen, J. Wölk, and R. Strey, J. Chem. Phys. **132**, 244505 (2010).

[28]I. J. Ford, Phys.Rev. E **56**, 5615 (1997).
[29]I. Kusaka, A. -G. Wang, and J. H. Seinfeld, J. Chem. Phys. **108**, 3416 (1998).
[30]K. Yasuoka and M. Matsumoto, J. Chem. Phys. **109**, 8451 (1998).
[31]K. Yasuoka and M. Matsumoto, J. Chem. Phys. **109**, 8463 (1998).
[32]P. R. ten Wolde and D. Frenkel, J. Chem. Phys. **109**, 9901 (1998).
[33]P. R. ten Wolde, M. J. Ruiz-Montero and D. Frenkel, J. Chem. Phys. **110**, 1591 (1999).
[34]K. J. Oh and X. C. Zeng J. Chem. Phys. **110**, 4471 (1999).
[35]I. Kusaka and D. W. Oxtoby, J. Chem. Phys. **110**, 5249 (1999).
[36]B. Senger, P. Schaaf, D.S. Corti, R. Bowles, D. Pointu, J. -C. Voegel, and H. Reiss, J. Chem. Phys. **110**, 6438 (1999).
[37]K. J. Oh and X. C. Zeng J. Chem. Phys. **112**, 294 (2000).
[38]S. Tanimura, K. Yasuoka, and T. Ebisuzaki, J. Chem. Phys. **112**, 3812 (2000).
[39]H. Vehkamäki and I. J. Ford, J. Chem. Phys. **112**, 4193 (2000).
[40]K. Laasonen, S. Wonczak, R. Strey, and A. Laaksonen, J. Chem. Phys. **113**, 9741 (2000).
[41]P. Schaaf, B. Senger, J. -C. Voegel, R. K. Bowles, and H. Reiss, J. Chem. Phys. **114**, 8091 (2001).
[42]S. Yoo, K. J. Oh and X. C. Zeng J. Chem. Phys. **115**, 8518 (2001).
[43]S. Toxvaerd, J. Chem. Phys. **115**, 8913 (2001).
[44]B. Chen, J. I. Siepmann, K. J. Oh and M. L. Klein, J. Chem. Phys. **115**, 10903 (2001).
[45]S. Toxvaerd, J. Chem. Phys. **119**, 10764 (2003).
[46]K. K. Tanaka, H. Tanaka, K. Kawamura, and K. Nakazawa, J. Chem. Phys. **122**, 184514 (2005).
[47]H. Matsubara, T. Koishi, T. Ebisuzaki, and K. Yasuoka, J. Chem. Phys. 127, 214507 (2007).
[48]K. K. Tanaka, H. Tanaka, T. Yamamoto, and K. Kawamura, J. Chem. Phys. **134**, 204313 (2011).
[49]J. Diemand, R. Angelil, K. K. Tanaka, and H. Tanaka, J. Chem. Phys. **139**, 074309 (2013).
[50]D. Reguera, R. K. Bowles, Y. Djikaev, and H. Reiss, J. Chem. Phys. **118**, 340 (2003).
[51]D. Reguera, and H. Reiss, Phys. Rev. Let. **93**, 165701 (2004).
[52]V. I. Kalikmanov, J. Chem. Phys. **124**, 124505 (2006).
[53]J. Wedekind, J. Wölk, D. Reguera, and R. Strey, J. Chem. Phys. **127**, 154515 (2007).
[54]J. Merikanto, E. Zapadinsky, A. Lauri, I. Napari, and H. Vehkamäki, J. Chem. Phys. **127**, 104303 (2007).
[55]V. I. Kalikmanov, J. Wölk, and T. Kraska, J. Chem. Phys. **128**, 124506 (2008).
[56]H. J. Berendsen, J. R. Grigera. and T. P. Straatsma, J. Chem. Phys. **91**, 6269 (1987).
[57]F. Zipoli, T. Laino. S. Stolz, E. Martin, C. Winkelmann, and A. Curioni, J. Chem. Phys. **139**, 094501 (2013).
[58]R. Schulz, B. Lindner, L. Petridis, and J. C. Smith, J. Chem. Theory Comput. **5**, 2798 (2009).
[59]W. L. Jorgensen, D. S. Maxwell, and J. Tirado-Rives, J. Am. Chem. Soc. **118**, 11225 (1996).
[60]K. K. Tanaka, J. Diemand, R. Angelil, and H. Tanaka, submitted.
[61]B. N. Hale, J. Chem. Phys. **122**, 204509 (2005).
[62]J. Qian, E. Stöckelmann, and R. Hentschke, J. Mol. Model **5**, 281 (1999).
[63]M. Matsumoto, Fluid Phase Equilib. **125**, 195 (1996).
[64]R. Angelil, J. Diemand, K. K. Tanaka, and H. Tanaka, J. Chem. Phys. **140**, 074303 (2014).

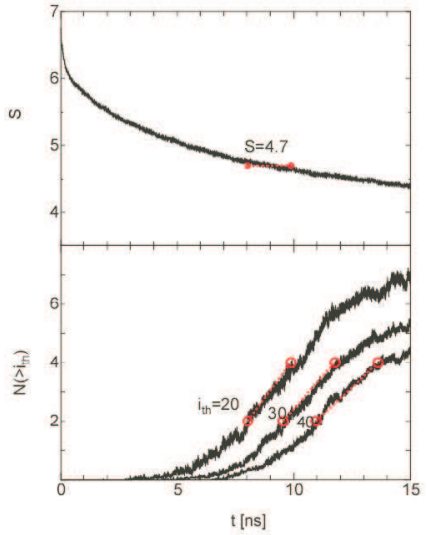


FIG. 1. Supersaturation ratio and number of clusters above various threshold sizes as a function of time for run 5d, where $N(> i_{\rm th})$ is averaged from 20 runs with the same initial conditions.

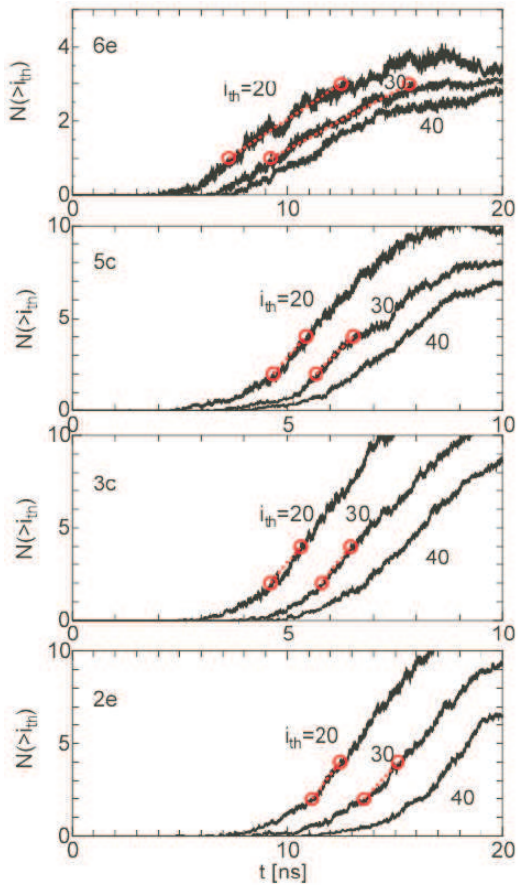


FIG. 2. Number of clusters above various threshold sizes as a function of time for various runs, where $N(> i_{\rm th})$ is averaged from 20 runs with the same initial conditions.

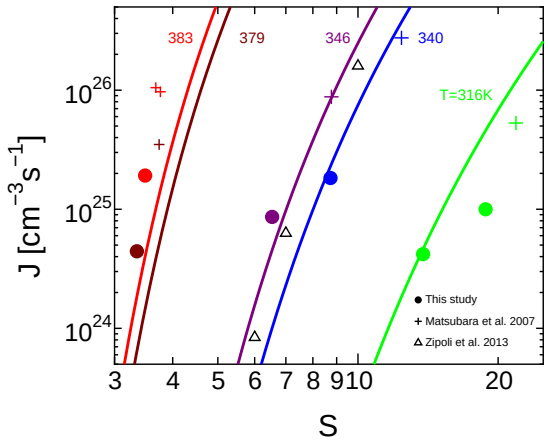


FIG. 3. The nucleation rates obtained by the MD simulations as a function of the supresaturation ratio for various temperatures. The previous results are also shown: crosses and triangles are the results by Matsubara et al.[47] and Zipoli et al.[57], respectively. In Zipoli et al.[57], we use the nucleation rates at 350 K. The nucleation rates by SP model (solid curve) are also plotted.

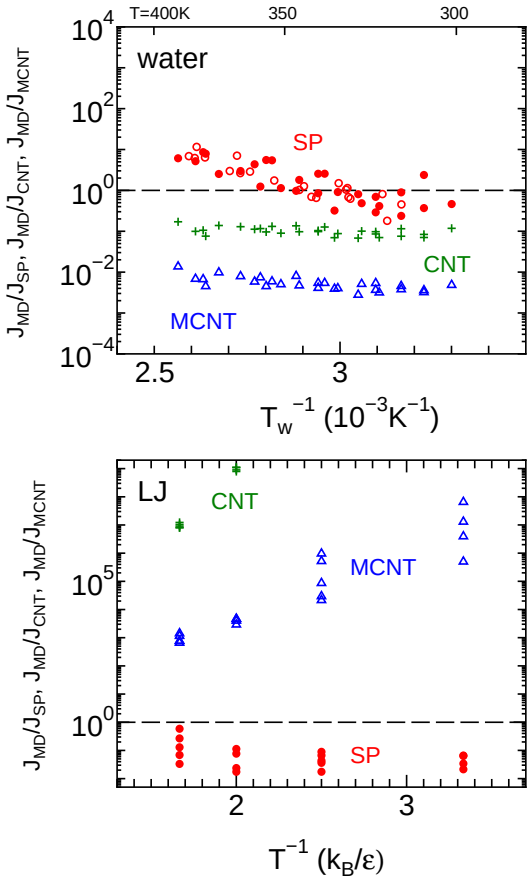


FIG. 4. The top panel shows the results for water obtained in this study. The ratios of nucleation rates of our MD simulations and the theoretical models, plotted with closed circles for the SP model ($J_{\rm MD}/J_{\rm SP}$), triangles for the MCNT ($J_{\rm MD}/J_{\rm MCNT}$), and crosses for the CNT ($J_{\rm MD}/J_{\rm CNT}$). The temperature is $T_{\rm w}$. By using $J_{\rm MD}$ obtained by Matsubara et al[47], we also plot $J_{\rm MD}/J_{\rm SP}$ with open circles. The results of the Lennard-Jones system[48] are also shown in the bottom panel for reference.

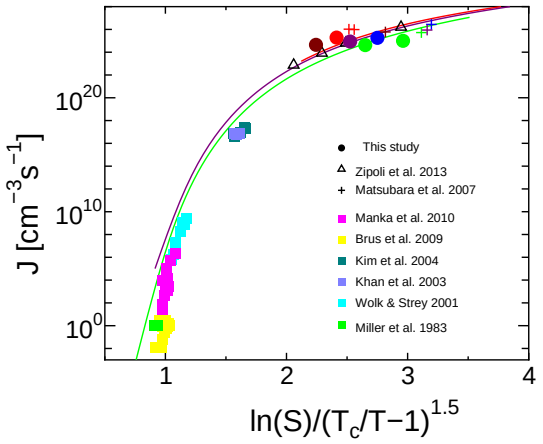


FIG. 5. The nucleation rates as a function of $\ln S/(T_c/T-1)^{1.5}$. The data by the MD simulations and the theoretical predictions by the SP model (316 K, 346 K, and 383 K) are the same as those in Fig. 3. For the MD simulations using SPC/E water model, we set $T_c = 630$ K[47]. We also put the experimental data for nucleation of water by Miller et al.[6], Wölk and Strey[20], Khan et al.[22], Kim et al.[23], Brus et al.[26], and Manka et al.[27]. For the experimental results and Zipoli et al.[57], T_c is set to be 647 K[20].

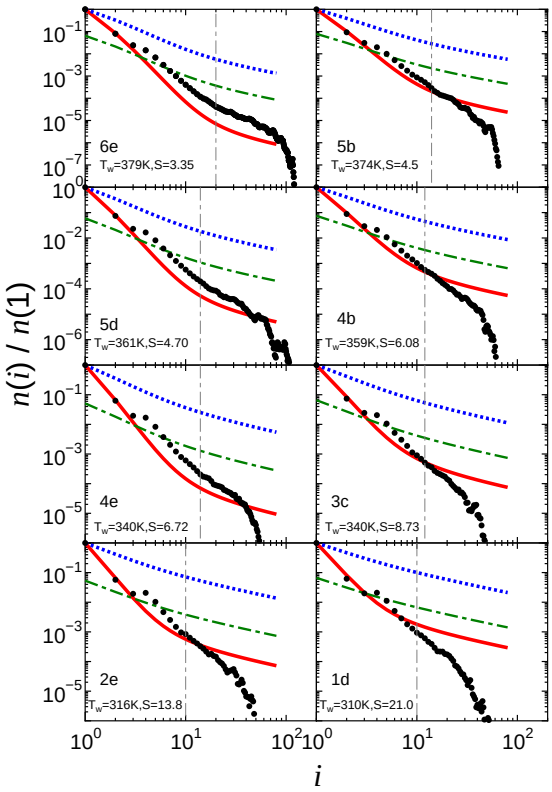


FIG. 6. The size distribution of clusters $n(i)$ obtained by the MD simulations is indicated by closed circles for the typical case. The size distributions obtained by the SP model (solid curve), the MCNT (dotted curve), and the CNT (dotted-dashed curve) are also plotted. The dotted-dashed lines show the size of critical clusters evaluated by the MD simulations.

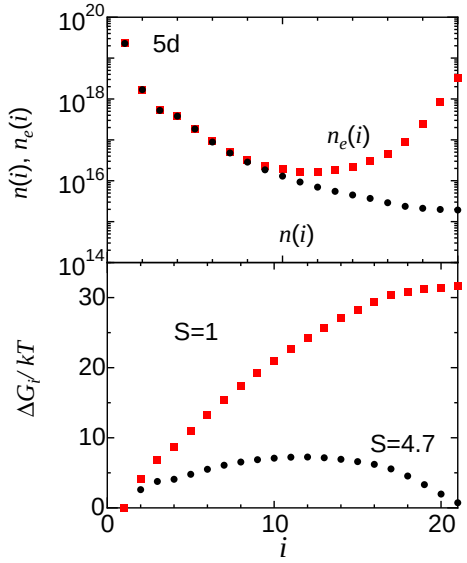


FIG. 7. The size distribution of clusters obtained by MD simulations (filled circles) and the equilibrium one (filled squares) in run 5d are shown in the top panel. In the bottom panel, the formation free energies of a cluster $\Delta G_i(S=1)/kT$ are shown for $S=4.7$ (filled circles) and $S=1$ (filled squares).

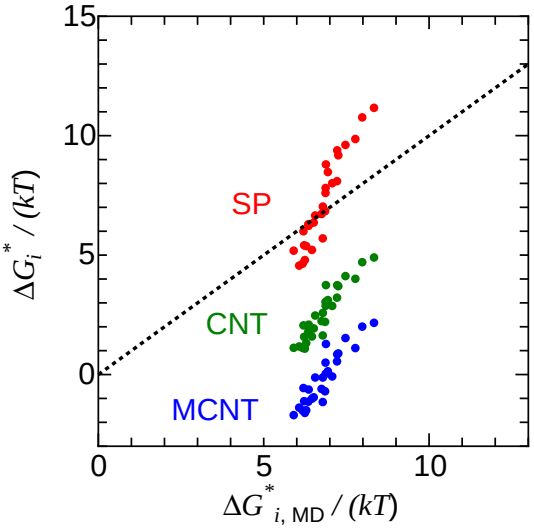


FIG. 8. The comparison of the maximum values of the formation free energy obtained by theoretical models and MD simulations $\Delta G^*_{\mathrm{i,MD}}$.

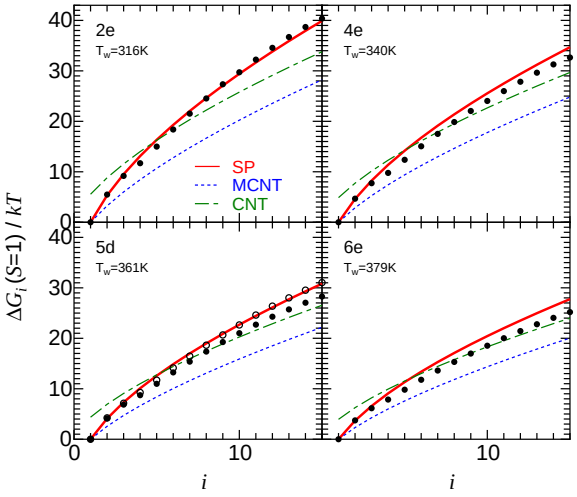


FIG. 9. The formation free energy of a cluster $\Delta G_i(S = 1)/kT$ at various temperatures is shown by the filled circles. $T_{\rm w} = 316$ K (run 2e), 340 K (4e), 361 K (5d), and 379 K (6e). The values obtained by the SP model (solid lines), the MCNT (dotted lines), and the CNT (dotted-dashed lines) are also shown. In run 5d, we also plotted the results of $T_{\rm w} = 359$K (run 4b) with open circles.

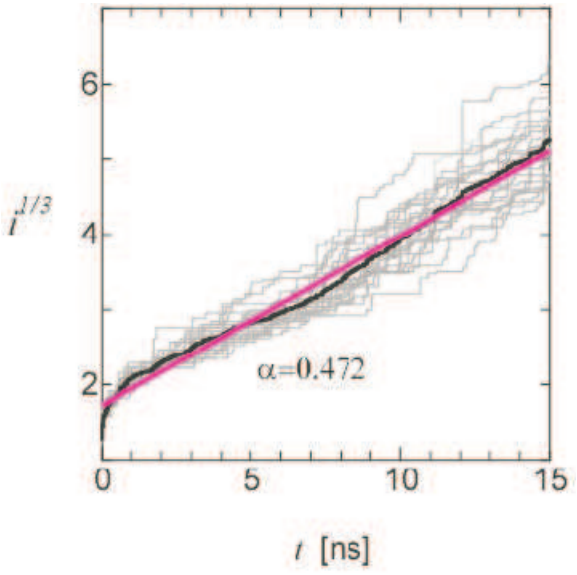


FIG. 10. Time evolution of the size of the largest cluster for 20 runs of 5d. The average value is plotted by a black line. Based on the averaged slope (red line), the sticking probability was found to be 0.472.

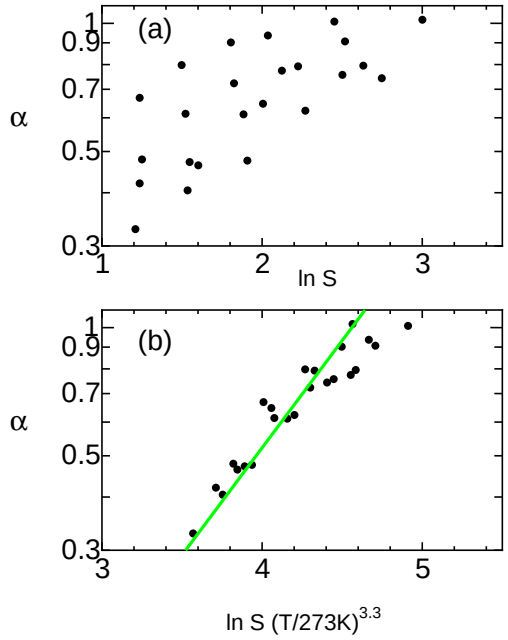


FIG. 11. (a) The sticking probabilities obtained by MD simulations as a function of supersaturation. (b) The sticking probabilities as a function of $\ln S(T/273\mathrm{K})^{3.3}$ The equation of the line of best fit is $\ln \alpha = 1.16 \ln S(T/273\mathrm{K})^{3.3} - 5.3$, which is shown by a solid line.

TABLE I. Parameters in the MD simulations, temperature of carrier gas T, cell size L, initial number density of monomers $n(1)_{t=0}$, number of carrier gas $N_{\rm cg}$, and simulation time $t_{\rm end}$.

run#	T [K]	L[nm]	$n(1)_{t=0}$[10^{-2}nm^{-3}]	$N_{\rm cg}$	$t_{\rm end}$ [ns]
6e	375	44.10	4.66	4000	20
6d	375	42.30	5.28	4000	15
6c	375	40.50	6.02	4000	10
6b	375	36.82	8.01	4000	8
5e	350	52.50	2.76	4000	30
5e2	350	52.50	2.76	8000	30
5d	350	49.50	3.30	4000	15
5c	350	45.00	4.39	4000	10
5b	350	40.91	5.84	4000	8
4e	325	59.90	1.86	4000	20
4e2	325	59.90	1.86	8000	20
4d	325	54.45	2.48	4000	15
4c	325	49.50	3.30	4000	10
4b	325	45.00	4.39	4000	8
3e	300	65.34	1.43	4000	20
3e2	300	65.34	1.43	8000	20
3d	300	59.40	1.91	4000	15
3c	300	54.00	2.54	4000	10
3b	300	49.09	3.38	4000	8
2e	275	70.79	1.13	4000	20
2e2	275	70.79	1.13	8000	20
2d	275	64.35	1.50	4000	15
2c	275	58.50	2.00	4000	10
v2b	275	53.18	2.66	4000	8
1e	250	76.23	0.903	4000	20
1d	250	69.30	1.20	4000	15
1c	250	63.00	1.60	4000	10
1b	250	57.27	2.13	4000	8

TABLE II. Summary of the results of the MD simulations. T [K]: temperature of carrier gas, $T_{\rm w}$ [K]: temperature of water molecules, S: averaged supersaturation ratio in the nucleation stage, $J_{\rm MD}[10^{24}\ {\rm cm}^{-3}{\rm s}^{-1}]$: nucleation rates obtained by the MD simulations, $J_{\rm SP}[10^{24}{\rm cm}^{-3}{\rm s}^{-1}]$: nucleation rates by the SP model, $J_{\rm MCNT}[10^{24}{\rm cm}^{-3}{\rm s}^{-1}]$: nucleation rates by the MCNT , $J_{\rm CNT}[10^{24}{\rm cm}^{-3}{\rm s}^{-1}]$: nucleation rates by the CNT , i^*: critical cluster size evaluated by the MD simulations, $i^*_{\rm SP}$: critical cluster size evaluated by the SP model, $i^*_{\rm CNT}$: critical cluster size evaluated by the CNT (or MCNT) model, and α: sticking probability.

run#	T	$T_{\rm W}$	S	$J_{\rm MD}$	$J_{\rm SP}$	$J_{\rm MCNT}$	$J_{\rm CNT}$	i_*	$i_{*,{\rm SP}}$	$i_{*,{\rm CNT}}$	α
6e	375	379	3.35	4.44±0.82	0.563	985	58.4	14	20	10	0.328
6d	375	380	3.37	9.74±1.6	1.13	1461	92.1	14	19	10	0.425
6c	375	383	3.49	19.2±2.3	3.71	2811	193.1	13	17	9	0.479
6b	375	390	3.41	83.7±19.0	13.7	6116	490.8	12	16	8	0.671
5e	350	357	4.61	3.71±0.65	0.67	822.1	38.5	13	15	7	0.407
5e-2	350	355	4.98	7.03±3.0	1.29	1189	53.5	11	14	6	0.464
5d	350	361	4.70	8.92±1.5	2.05	1530	79.5	12	14	7	0.472
5c	350	366	4.78	29.1±3.9	9.77	3684	224.7	14	13	6	0.609
5b	350	374	4.50	68.7±9.6	27.2	7015	497.0	13	12	6	0.798
4e	325	340	6.72	3.73±0.8	1.46	911	38.0	11	11	5	0.476
4e-2	325	338	7.28	5.94±0.3	2.32	1099	46.7	12	10	5	0.649
4d	325	346	6.54	8.63±0.5	4.79	1837	88.6	12	11	5	0.613
4c	325	352	6.48	19.1±4.3	16.8	3805	213	11	10	4	0.719
4b	325	359	6.08	49.1±9.8	39.6	6630	422	11	10	4	0.904
3e	300	328	10.0	2.99±0.4	3.7	1076	43.9	10	9	4	0.622
3e-2	300	323	11.8	4.92±0.5	7.08	1347	57.3	10	8	3	0.762
3d	300	334	9.09	7.42±0.3	8.14	1845	84.7	11	9	4	0.794
3c	300	340	8.73	18.3±0.57	21.5	3369	175.8	9	8	3	0.776
3b	300	347	7.99	46.6±21	47.8	5813	343	10	8	3	0.938
2e	275	316	13.8	4.20±0.60	4.69	921.8	36.4	9	7	3	0.748
2e-2	275	310	18.6	4.50±0.60	12.2	1254	53.7	10	6	2	1.02
2d	275	322	13.4	5.59±1.1	13.5	1766	79.6	11	7	3	0.803
2c	275	327	12.7	16.1±4.7	33.2	3144	160	10	7	3	0.911
2b	275	335	11.2	20.0±4.3	62.4	5113	287	11	7	3	1.02
1e	250	303	23.0	4.39±2.0	9.47	908	37.2	9	6	2	0.885
1d	250	310	21.0	5.22±0.95	2.19	1623	74.1	10	6	2	0.927
1c	250	316	18.8	10.0±1.4	42.1	2644	132	10	6	2	1.01
1b	250	323	16.3	24.0±3.1	82.6	4472	246	10	6	2	1.12